4. *PAPER III*: *S*-ADENOSYL-L-METHIONINE:MAGNESIUM-PROTOPORPHYRIN IX *O*-METHYLTRANSFERASE FROM *RHODOBACTER CAPSULATUS*: MECHANISTIC INSIGHTS AND STIMULATION WITH PHOSPHOLIPIDS

4.1 Synopsis

- Kinetically characterized *S*-adenosyl-L-methionine:magnesium-protoporphyrin IX *O*-methyltransferase from *Rba. capsulatus*
- Developed a heterologous expression and purification method for BchM
- Discovered there was a phospholipid requirement for BchM stability and optimal *O*-methyltransferase activity
- Determined kinetic constants (K_m and K_i) of substrates and product inhibitors respectively and proposed a reaction mechanism for *O*-methyltransferase
- There was no stimulatory effect of magnesium chelatase subunits upon *O*-methyltransferase activity

4.2 Journal article

Paper III

This research was originally published in Biochemical Journal, **Sawicki A, Willows RD** (2007) *S*-Adenosyl-L-methionine:magnesium-protoporphyrin IX *O*-methyltransferase from *Rhodobacter capsulatus*: mechanistic insights and stimulation with phospholipids. Biochem. J. **406:** 469-478, http://www.biochemj.org

BJ www.biochemj.org

BJ Structure

Biochem. J. (2007) **406**, 469–478 (Printed in Great Britain) doi:10.1042/BJ20070284

online data

S-Adenosyl-L-methionine:magnesium-protoporphyrin IX *O*-methyltransferase from *Rhodobacter capsulatus*: mechanistic insights and stimulation with phospholipids

Artur SAWICKI and Robert D. WILLOWS[1]

Department of Chemistry and Biomolecular Sciences, Macquarie University, Sydney, NSW 2109, Australia

The enzyme BchM (*S*-adenosyl-L-methionine:magnesium-protoporphyrin IX *O*-methyltransferase) from *Rhodobacter capsulatus* catalyses an intermediate reaction in the bacteriochlorophyll biosynthetic pathway. Overexpression of His_6-tagged protein in *Escherichia coli* resulted in the majority of polypeptide existing as inclusion bodies. Purification from inclusion bodies was performed using metal-affinity chromatography after an elaborate wash step involving surfactant polysorbate-20. Initial enzymatic assays involved an *in situ* generation of *S*-adenosyl-L-methionine substrate using a crude preparation of *S*-adenosyl-L-methionine synthetase and this resulted in higher enzymatic activity compared with commercial *S*-adenosyl-L-methionine. A heat-stable stimulatory component present in the *S*-adenosyl-L-methionine synthetase was found to be a phospholipid, which increased enzymatic activity 3–4-fold. Purified phospholipids also stabilized enzymatic activity and caused a disaggregation of the protein to lower molecular mass forms, which ranged from monomeric to multimeric species as determined by size-exclusion chromatography. There was no stimulatory effect observed with magnesium–chelatase subunits on methyltransferase activity using His–BchM that had been stabilized with phospholipids. Substrate specificity of the enzyme was limited to 5-co-ordinate square-pyramidal metalloporphyrins, with magnesium-protoporphyrin IX being the superior substrate followed by zinc-protoporphyrin IX and magnesium-deuteroporphyrin. Kinetic analysis indicated a random sequential reaction mechanism. Three non-substrate metalloporphyrins acted as inhibitors with different modes of inhibition exhibited with manganese III-protoporphyrin IX (non-competitive or uncompetitive) compared with cobalt II-protoporphyrin IX (competitive).

Key words: bacteriochlorophyll biosynthesis, BchM, magnesium–chelatase, methyltransferase, phosphatidylglycerol, *Rhodobacter capsulatus*.

INTRODUCTION

The photosynthetic bacterium *Rhodobacter capsulatus* is an example of a facultative photoheterotroph that uses photosynthesis as an energy source under anaerobic conditions in the light [1]. The bacteriochlorophyll biosynthetic pathway is required for photosynthetic growth, and mutational analysis with *R. capsulatus* was previously carried out to determine the intermediates and genetic loci of the enzymes involved [2–6]. This allowed the photosynthetic gene cluster to be assembled [7] (EMBL accession number Z11165). The genetic locus *bchM* was found to encode the BchM (*S*-adenosyl-L-methionine:magnesium-protoporphyrin IX *O*-methyltransferase) [8–10]. Details of the enzymatic steps including the genes involved from aminolevulinic acid, derived from glutamate, to (bacterio)chlorophyll can be found in previously published reviews [11–14].

The enzyme BchM (EC 2.1.1.11) catalyses the methylation of a carboxyl group of Mg-proto (magnesium-protoporphyrin IX) by the ubiquitous methylating agent SAM (*S*-adenosyl-L-methionine), yielding MgPE (magnesium-protoporphyrin IX monomethyl ester) and SAH (*S*-adenosylhomocysteine) [15]. The homologous enzyme in plants is called ChlM and the porphyrin substrate and product are important signalling molecules in plastid–nucleus communication in plants. A mutant of ChlM in *Arabidopsis*, that accumulated Mg-proto had a negative impact on photosystem gene expression [16] and the effect of Mg-proto and MgPE as a way of co-ordinating chlorophyll biosynthesis with photosystem assembly was reviewed recently [17]. Methyltransferase has been studied kinetically in some detail from plants, algae and photosynthetic bacteria with K_m values in the range 20–230 μM for SAM and 10–48 μM for Mg-proto [18–27], although K_m for Mg-proto using *Rhodobacter spheroides* was not determined since it approached zero [22]. Most of the studies on the bacterial and plant enzyme were undertaken before nucleotide sequence information was available and therefore crude or partially purified protein was used. With the *R. capsulatus* gene sequences being identified, heterologous expression of BchM from *R. spheroides* and *R. capsulatus* in *E. coli* was possible with demonstration of enzymatic activity [9,10]. The ChlM protein from *Synechocystis* PCC 6803 complemented a BchM mutant of *R. capsulatus* [28]. Most recently *Synechocystis* PCC 6803 ChlM has been heterologously expressed in *E. coli* and purified to homogeneity [25].

The reaction mechanism of methyltransferase appears to vary between a plant, algal and photosynthetic bacterium. The wheat enzyme exhibited a ping-pong mechanism with SAM binding first [19,27], whereas a random sequential mechanism was elucidated for *Euglena gracilis* [23] and *Synechocystis* [25]. An ordered sequential mechanism was determined for *R. spheroides* with Mg-proto obligated to bind to the enzyme first [22].

Methyltransferase is mainly associated with membranes according to differentiation of the cell fractions and measurement

Abbreviations used: BchM, *S*-adenosyl-L-methionine:magnesium-protoporphyrin IX *O*-methyltransferase; DOPG, dioleoyl $(C_{18:1})_2$ phosphatidylglycerol; DPPG, dipalmitoyl $(C_{16:0})_2$ phosphatidylglycerol; DTT, dithiothreitol; HisBchM, His_{16}-tagged BchM; Mg-deutero, magnesium-deuteroporphyrin; Mg-proto, magnesium-protoporphyrin IX; MgPE, magnesium-protoporphyrin IX monomethyl ester; pe, phosphatidylethanolamine; pg, phosphatidylglycerol; POPG, palmitoyl-oleoyl $(C_{18:1,16:0})$ phosphatidylglycerol; SAH, S-adenosylhomocysteine; SAM, *S*-adenosyl-L-methionine.

[1] To whom correspondence should be addressed (email rwillows@rna.bio.mq.edu.au).

of enzymatic activity. It was detergent solubilized from barley chloroplast membranes [26], located on membrane fragments from chromatophores in *R. spheroides* [20], membrane-bound and soluble in *E. gracilis* [29] and associated with chloroplast envelope and thylakoid membrane in spinach and *Arabidopsis thaliana* [30]. A soluble form of the enzyme was obtained using sucrose and crude wheat homogenates [18]. Amino acid analysis of *A. thaliana* and *Oriza sativa* revealed two putative transmembrane domains at the same location in each plant sequence with the N-terminal portion suspected of being membrane-associated. This N-terminal region is not present in bacterial sequences and there is an independent putative transmembrane region near the C-terminus [30].

There is indirect and direct evidence to suggest that there is an interaction between methyltransferase and magnesium–chelatase (E.C. 6.6.1.1). The latter is a multisubunit enzyme involved in the previous step of the bacteriochlorophyll biosynthetic pathway, magnesium-insertion into protoporphyrin IX [31,32]. It is ATP-dependent (AAA protein) [33] and is comprised of the subunits BchI (approx. 40 kDa), BchD (approx. 70 kDa), and BchH 9 (approx. 140 kDa) [34]. An interaction of BchM and magnesium–chelatase was first suggested 35 years ago by Gorchein [35], based on *in vivo* studies using *R. spheroides*. Exogenous protoporphyrin IX fed into cells showed the accumulation of MgPE. The addition of ethionine (converted into *S*-adenosylethionine *in vivo*), which is a competitive inhibitor of SAM-dependent methyltransferases [20] exhibited no accumulation of Mg-proto [35]. A build-up of Mg-proto is expected if the magnesium–chelatase and BchM enzymes were acting independently. More recently it was observed that the membrane fraction of heterologously expressed BchM from *R. capsulatus* supplemented with a soluble BchH fraction stimulated methyltransferase activity [36]. Although there was no observed stimulatory effect of purified *Synechocystis* ChlH on ChlM activity, there was increased activity using crude lysates of co-expressed magnesium–chelatase subunits ChlI, D, H and ChlM compared with ChlM alone [37]. Using purified protein, it was later found that the ChlH stimulatory effect is observed in a much shorter time period (milliseconds) using quenched flow techniques [38] compared with the previous 30 min stopped assay [37]. This contrasts with the study in which the heterologously expressed tobacco ChlM was significantly stimulated with expressed ChlH in similar minute-scale assays [39]. There is a correlation between the transcription and expression of tobacco methyltransferase and magnesium–chelatase with increased transcript and protein levels of methyltransferase together with magnesium–chelatase ChlH subunit in *ChlM* sense transgenic plants and a suppressed level of magnesium–chelatase ChlH-subunit together with methyltransferase in *ChlM* antisense tobacco plants [40].

The properties of the methyltransferase, using HisBchM (His_6-tagged BchM), presented here show a previously unreported lipid requirement for optimal activity and the kinetic data reveal some new insights into the reaction mechanism and the nature of substrate binding. In addition we also re-examine the reported stimulation of methyltransferase activity by magnesium–chelatase using purified HisBchM with magnesium–chelatase subunits, BchI, HisBchD and HisBchH.

EXPERIMENTAL

Materials

Unless stated elsewhere all chemicals were obtained from Sigma–Aldrich, Ajax Finechem, Astral Scientific, APS Finechem, Calbiochem, Selby-Biolab, BDH chemicals and J.T. Baker. Growth medium was from Difco Laboratories. Surfactant polysorbate P-20 (P-20) was from Biacore AB (Uppsala, Sweden). Protoporphyrin IX, deuteroporphyrin, and hemin were from Porphyrin Products (Logan, UT, U.S.A.). Protein determinations were performed with a Bio-Rad protein assay reagent according to the manufacturer's instructions with BSA as a standard [41].

Cloning, expression and purification of proteins

Magnesium–chelatase subunits BchD and BchH were expressed and purified as their His_6-tagged products (HisBchD and HisBchH), whereas BchI was purified as the native form as described previously [42]. SAM synthetase (E.C. 2.5.1.6) from the overproducing *E. coli* strain DM22pK8 [44] was partially purified using ammonium sulfate precipitation [45] and dialysed against 100 mM Tris/HCl (pH 8.0), 10 % (v/v) glycerol, 1 mM EDTA and 0.1 % 2-mercaptoethanol at 5 °C for 4 h, and then stored at − 80 °C. BchM from *R. capsulatus* was heterologously expressed in *E. coli*. The plasmid pRPS404 [6], consisting of a 46 kb pair section of the *R. capsulatus* photosynthetic gene cluster [7], was used as a PCR template using the Eppendorf Triplemaster PCR system with the following primers: 5′-TCATGCCCGATACTCCAGGCATTC-3′ and 5′-CACCATGCCCTCCGATTACGCAGAGATC-3′. The expression plasmid pHisBchM was obtained by directly cloning this PCR product into a pET 100/D-TOPO vector (Invitrogen) and the fidelity of the construct was confirmed by DNA sequencing using the Dye termination method with an ABI Prism model 377 automated fluorescent DNA sequencer (Perkin–Elmer). *E. coli* (BL21DE3) Star strain containing this plasmid was used for expression of HisBchM in Luria–Bertani medium with 100 μg/ml ampicillin. The cells were grown at 37 °C to a D_{600} of 0.3–0.5 when the flask was cooled to 18 °C and induced for 13–18 h with 0.25 mM isopropyl β-D-thiogalactopyranoside. Cells were harvested by centrifugation at 8000 ***g*** for 15 min at 4 °C, and then resuspended in binding buffer (20 mM Tris/HCl, pH 7.9, 0.5 M NaCl and 5 mM imidazole). The cells were lysed using a Thermospectronic French Press at approximately 7×10^4 kPa and centrifuged for 30 min at 30000 ***g*** at 4 °C. The pellet was washed with distilled water and re-centrifuged and the supernatant was discarded. Enzymatically active HisBchM protein was extracted from the pellet with solubilization buffer [20 mM Tricine/NaOH, pH 8.2, 1 M KCl, 0.05 % P-20 and 1 mM DTT (dithiothreitol)], and re-centrifuged. The supernatant was named the soluble fraction. The pellet was dissolved in solubilization buffer containing 6 M Guanidine/HCl, re-centrifuged and this supernatant was named the Guanidine-soluble fraction. Purification of HisBchM from the soluble fraction was performed in a single step as described in the pET system manual (Invitrogen) using a HiTrap Ni^{2+} FF chelating column (GE Healthcare BioSciences) with the following modifications: wash steps contained increasing imidazole concentrations, of 5, 60 and 100 mM in 20 mM Tris/HCl (pH 7.9), 0.5 M NaCl, 0.5 M KCl and 1 mM DTT, and used two column volumes for each. HisBchM was eluted by 500 mM imidazole and the above buffer components (elution buffer). Phosphatidylglycerol was added to a final concentration of 25–50 μg/ml and HisBchM was desalted into 50 mM Tricine/NaOH (pH 8.2), 10 % (v/v) glycerol and 1 mM DTT with a NAP-10 column (GE Healthcare BioSciences). Purified protein was concentrated using a 10 kDa cut-off membrane (Millipore) by centrifugation at 4000 ***g*** for 15 min at 4 °C, and to give final concentrations of approx. 0.2–4.5 μg/μl with approximately similar phosphatidylglycerol concentrations. If the concentrated protein was turbid, the solution was clarified by centrifugation at 18000 ***g*** for 5 min at room temperature, and the pellet discarded. The supernatant was stored

in assay-size aliquots at −80 °C with the activity retained for at least 3 months. The Guanidine-soluble fraction was purified as above with 6 M Guanidine/HCl present in the wash steps. Refolding was performed with stepwise reduction of Guanidine/HCl in binding buffer (two column volumes each) from 6 M, 3 M, 1 M, 0.5 M, to 0 M. The protein was eluted as described above with elution buffer and the desalting and concentration steps performed as for the soluble fraction. SDS/PAGE was performed according to the method of Schägger and von Jagow [45a] using 4–20 % gradient gels (LifeGels) at 150 V, and the gel was stained with Coomassie Brilliant Blue.

Metalated magnesium, nickel, copper, zinc, cobalt and manganese protoporphyrin IX, and magnesium-deuteroporphyrin synthesis and purification

Synthesis of Mg-proto dipotassium salt was performed based on the method of Fuhrhop and Granick [46]. Other metal protoporphyrins were based on a modified method stated in Falk [47] using the metal acetates: nickel, copper, zinc, cobalt and magnesium with pyridine or glacial acetic acid as the solvent. The metalated porphyrins were precipitated with ice-cold water generally (one part pyridine or acetic acid to 5–10 parts water) and collected by centrifugation at 5000 ***g*** for 15 min at 4 °C. The precipitate was washed a further five times with water to remove most of the pyridine, and the final precipitate was dried under nitrogen flow, desiccated over silica beads for several days and stored at −20 °C. The synthesis of Mg-deutero (magnesium-deuteroporphyrin) was carried out in the same way as for Mg-proto, and the precipitation/drying stage was the same as for the other metal protoporphyrins. Metalloporphyrin stock solutions were newly prepared for each assay by dissolving a speck of solid in 1 μl of 1 M NaOH and adding 100–1000 μl water with concentrations determined using the appropriate solvent and molar extinction coefficients for Ni-, Cu-, Zn-, Co- and Mn-proto [48] or ε_{408} 278000 $M^{-1} \cdot cm^{-1}$ for Mg-proto, ε_{398} 433000 $M^{-1} \cdot cm^{-1}$ for Mg-deutero [49] and ε_{400} 90000 $M^{-1} \cdot cm^{-1}$ for hemin [50].

Mn(III), Co(III) and Fe(III) metalloporphyrins were reduced to Mn(II), Co(II) and Fe(II) forms under basic conditions [51] using 1 mM NaOH, 159 μM POPG [palmitoyl-oleoyl($C_{18:1,16:0}$)-phosphatidylglycerol] and 960 mM sodium dithionite. Spectral changes were observed in the visible absorbance region and the reduced metalloporphyrins did not re-oxidize when diluted in assay buffer (50 mM Tricine/NaOH, pH 8.0, and 1 mM DTT).

MgPE enzymatic synthesis

Synthesis of MgPE was performed on a 200 ml scale with the following components: 50 mM Tricine/NaOH (pH 8.0), 1 mM DTT, 1.8 mM $MgCl_2$, 1.3 mM ATP, 3 mM KCl, 8.8 mM glycerol, 2 μM Mg-proto, 0.4 mM L-methionine, 0.18 mg crude SAM synthetase and 0.2–0.6 μM partially purified HisBchM (from cell lysate supernatant) at 30 °C with gentle agitation. The formation of MgPE was monitored periodically by HPLC until complete conversion was achieved (typically 3–4 h) and the sample was lyophilized. Extraction of MgPE was performed according to the method of Ellsworth and Murphy [52]. MgPE was applied as an aqueous extract to a Waters C18 Sep-pak Plus column which was washed in a step-wise fashion with 5 ml each of 10 %, 20 %, 30 % and 35 % (v/v) acetonitrile. MgPE was finally eluted by 45–80 % (v/v) acetonitrile (typically 5–10 ml), and checked for purity by HPLC (this was typically ⩾99 % by Abs/fluorescence) and the solution lyophilized. MgPE stocks for assays were initially dissolved in 2 % (v/v) ethanol, 1 mM NH_3, and centrifuged repeatedly for 5 min at room temperature (20 °C) at 18000 *g* until no pellet was observed, and this supernatant was used for inhibition assays.

Phospholipid preparation for assays

Crude bacterial phospholipids were extracted from BL21 (DE3) *E. coli* according to the method described by Osborn and Rothfield [53] and stored in 3:1 chloroform/methanol under nitrogen or argon in the dark at −80 °C. The concentration of the prepared phospholipids was based on the mass of a dried sample. The dried phospholipids were not used in the assays. Both crude and commercial phospholipids (Sigma) used in assays were prepared in aqueous solution as follows: a fraction of the phospholipids dissolved in chloroform/methanol was evaporated under nitrogen or argon flow to a volume of approx. 10 μl, then 4 volumes of methanol were added, evaporated again until approx. 10 μl remained. At least a 10 volume excess of water was then added, and the methanol evaporated again under nitrogen or argon flow to leave the phospholipids as a transparent aqueous micellar suspension. This suspension was sonicated for 20 min at room temperature, followed by centrifugation for 5 min at room temperature and 18000 ***g*** with this supernatant used for assays.

Methyltransferase enzymatic assays

Assays were in a total volume of 110–650 μl with final concentrations of 50 mM Tricine/NaOH (pH 8.0 or 8.2) or Tris/HCl (pH 8.5), 1 mM DTT and varying phospholipid, HisBchM, SAM and metalloporphyrin concentrations for 10 s to 30 min at 30 °C. Assays involving Co(III)-proto as the substrate contained no DTT. For exact details of assay conditions refer to relevant Figure and Table legends. Coupled assays with SAM synthetase also contained 3 mM KCl, 1.8 mM $MgCl_2$, 1.3 mM ATP and 2 μg crude SAM synthetase per 100 μl assay. Stock solutions of SAM *p*-toluenesulfonate salt were prepared by dissolving the solid in 10 mM HCl and measuring the concentration based on ε_{257} 14700 $M^{-1} \cdot cm^{-1}$ [54] and stored in aliquots at −80 °C. Purified HisBchM stock solutions were used once for each set of reactions and diluted into 50 mM Tricine/NaOH (pH 8.0/8.2) or Tris/HCl (pH 8.0/8.5) and 1 mM DTT (with phospholipid added if applicable), followed by SAM/porphyrin in 50 mM Tris/HCl or Tricine/NaOH and 1 mM DTT to start the assay. Assays were stopped by taking 125 μl aliquots from each assay mix and adding to 105 μl 80:20 (v/v) acetone/water, spiked with 20 μl deuteroporphyrin as an internal standard to a final concentration of 1.21 μM in each 250 μl stopped assay. The internal standard was used to check for any obvious discrepancies in the data. The assay tubes were centrifuged at 18000 ***g*** for 5 min at room temperature, and the supernatant was used for analysis by HPLC. Assays and extractions with acetone were performed in the dark or in dim light.

Assays involving HisBchH and HisBchM were performed essentially according to HisBchM enzymatic assays. Assays involving BchI and HisBchD involved refolding 1 μl of 61 μM HisBchD in 6 M urea, 50 mM Tricine/NaOH (pH 8.0) and 4 mM DTT by rapidly adding 577 μl (200 μl at a time) of 0.45 μM BchI in 50 mM Tricine/NaOH (pH 8.0) and 1 mM DTT, and either 0.54 mM $MgCl_2$, 3.8 mM $MgCl_2$ or 3.8 mM $MgCl_2$ and 1.01 mM ATP on ice for 2 h [42] with any variations stated in the Figure and Table legends.

CD spectroscopy

CD spectroscopy measurements were carried out with a Jasco J-810 Spectropolarimeter. Wavelengths scans were from

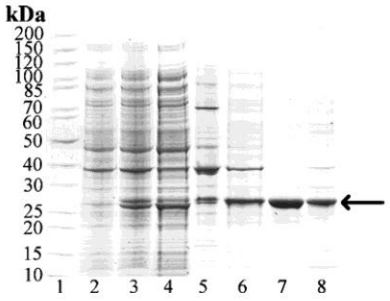

Figure 1 Expression and Ni^{2+}-affinity chromatography purification of HisBchM

Lane 1, Fermentas PageRuler protein ladder; lane 2, uninduced cells; lane 3, induced cells; lane 4, cell lysate inclusion body pellet; lane 5, cell lysate supernatant; lane 6, P-20 solubilized pellet; lane 7, 10 μg HiTrap FF purified HisBchM from P-20 solubilized pellet; lane 8, 8 μg HiTrap FF purified HisBchM from cell lysate supernatant. The arrow shows the band corresponding to the correct molecular mass of HisBchM (29.2 kDa).

190–300 nm at 100 nm/min using a 1 cm cuvette, with 1 nm bandwidth, 1 nm step size, 4 s response and 32 accumulations at 20 °C.

HPLC for analysing porphyrins

The HPLC method was modified from the method of Gibson and Hunter [10]. A Shimadzu HPLC system was used at 2 ml/min with an Alltech C8 column (150 × 4.6 mm), diode array detector and a Shimadzu RF-535 fluorescence detector. A gradient was used for separation of Mg-proto, Zn-proto and Mg-deutero with a 6 min linear gradient from 5 % buffer A water or 20 mM phosphate (pH 7.8) to 67 % buffer B (acetonitrile). The other metalloporphyrins used a 6 min linear gradient fom 5 % buffer A1; 0.1 M ammonium acetate (pH 6.8) to 90 % buffer B1; 48 % (v/v) acetonitrile, 48 % (v/v) methanol, 0.1 M ammonium acetate (pH 6.8). Then a 5 min gradient to 100 % buffer B1.

RESULTS AND DISCUSSION

Purification and optimization of HisBchM activity

HisBchM 29 kDa was purified as described in the Experimental section, as shown in Figure 1, and is prone to aggregation with the majority of expressed HisBchM protein as inactive aggregates or inclusion bodies (Figure 1, lane 5). Although active HisBchM was recovered by refolding from inclusion bodies the yield was very low and this fraction was not used further. Purification of HisBchM from the cell lysate supernatant using Ni^{2+}-affinity chromatography resulted in co-purification with other non-identified proteins (Figure 1, lane 8). This preparation was used in coupled HisBchM–SAM synthetase assays, characterizing the phospholipid effect, and synthesis of MgPE. The largest yields of active HisBchM, estimated at 98 % purity by SDS/PAGE (Figure 1, lane 7), were obtained by washing inclusion bodies with P-20 (Figure 1, lane 6) before application to the Ni^{2+}-affinity column, yielding approx. 0.5 mg of purified protein recovered from a 2 litre culture, which was used for experiments with magnesium–chelatase subunits, kinetics, substrate specificity and inhibition assays.

Some common detergents and simple alcohols were also tested to try and solubilise and further stabilise the HisBchM (Table 1).

Table 1 Effect of detergents and alcohols on HisBchM activity

Assays were for 10–20 min with the following concentrations of each component: 50 mM Tris/HCl (pH 8.5), 1 mM DTT, 2 μM Mg-proto and variable SAM and HisBchM concentrations as stated in the Table. The following concentration ranges were used: Tween 20 or P-20, 0.000003–0.05 % (v/v); dodecyl-β-D-maltoside, 0.004–4 % (w/v); alcohols, 0.06–10 % (v/v). Assays were compared with a control (assigned a value of 100 % activity) conducted in parallel.

Additive	Name	SAM (μM)	HisBchM (μM)	% Additive*	% Control
Detergents	Tween20	250	0.015	0.0004	117
	Dodecyl-β-D-maltoside	60	0.16	0.004	101
Surfactant	Polysorbate 20 (P-20)	250	0.015	0.0004	382
Alcohols	Methanol	62	0.2	1	90
	Ethanol	62	0.2	1	109
	Propanol	62	0.2	1	114
	Butanol	62	0.2	1	118

*Additives were used over a variety of concentrations with the optimal amounts stated here based on the greatest stimulatory effect.

P-20 at 0.0004 % (v/v) gave a 3.8-fold stimulatory effect on HisBchM activity, however it was unsuitable to help stabilize HisBchM as it aggregated when frozen. The other detergents tested, Tween-20 or dodecyl-β-D-maltoside, had no stimulatory effect at 0.0004 % (v/v) and 0.004 % (w/v) respectively. Several other detergents have been previously tested using *R. spheroides* chromatophores with mainly negative effects, albeit at relatively high detergent concentrations (0.5–1 %) [22]. A detergent concentration of 0.05 % (v/v) Tween-20 strongly inhibited purified HisBchM (in our experiments only 23 % of activity was retained). The straight chain alcohols (C_2, C_3 and C_4) had no stimulatory effect and were not inhibitory up to 1 % (v/v).

Coupled HisBchM–SAM synthetase assay and a stimulatory component

Preliminary HisBchM assays involved an *in situ* generation of SAM with crude SAM synthetase coupled with HisBchM. This approach gave a 1.4-fold higher relative activity compared with assaying HisBchM using commercial SAM. Surprisingly the addition of crude SAM synthetase to the HisBchM assay together with SAM resulted in up to a 4-fold increase in activity compared with SAM alone (Table 2). Crude BL21 (DE3) *E. coli* cell lysate supernatant also resulted in heightened HisBchM activity, which was retained after boiling, and the stimulatory component was larger than 5 kDa. It was speculated that the stimulatory effect was due to the phospholipid micelles. A preparation of a crude phospholipid extract from *E. coli* membranes also gave a comparable stimulatory effect.

Phospholipid effect on HisBchM activity

Specific phospholipid requirements have been found for many membrane proteins [55]; however, the stimulatory effect of crude preparations of phospholipids in our assays was labile as the stimulatory effect was lost after storage for 1 week. Therefore various commercial phospholipids with different polar head groups and alkyl chains (stable for several months at −80 °C in 99:1 chloroform/methanol) were tested for their stimulatory effect. Phospholipids were titrated to determine the optimal concentration that gave the highest stimulation of activity (for an example see Supplementary Figure 1 at http://www.BiochemJ.org/bj/406/bj4060469add.htm) and the results are shown in Table 3.

Table 2 Identification of stimulatory component of HisBchM activity

Crude phospholipids were prepared from *E. coli* as stated in the Experimental section. Assays were for 10 min using 50 mM Tris/HCl (pH 8.5), 1 mM DTT, 100 μM SAM and variable Mg-proto and HisBchM concentrations as stated in the Table. Assays were compared with a control (assigned a value of 100 % activity) conducted in parallel.

Additive	Mg-proto (μM)	HisBchM (μM)	Amount additive (μg)*	% Control
Crude SAM synthetase	0.1	0.0016	2	374 $\pm$ 25
E.coli BL21 supernatant	0.26	0.0017	4.2	321
Boiled crude SAM synthetase supernatant	0.26	0.0017	2	370 $\pm$ 17
Boiled *E.coli* BL21 supernatant	0.26	0.0017	4.2	350
< 5 kDa	0.28	0.0017	†	146 $\pm$ 19
> 5 kDa	0.28	0.0017	†	519 $\pm$ 71
BL21 *E.coli* crude phospholipids	0.27	0.001	0.6	355

*Additives were used over a variety of concentrations with the optimal amounts stated here based on the greatest stimulatory effect. Crude SAM synthetase assays were performed in duplicate, whereas *E. coli* BL21 supernatant and crude phospholipid were single assays. A strain of BL21 (DE3) Star *E. coli* was grown to stationary phase, lysed and centrifuged (60 min at 4 °C and 100 000 ***g***) and the supernatant used. The crude SAM synthetase and BL21 supernatant were boiled for 10 min, and re-centrifuged.

† 0.5 ml of a 2.5 mg/ml fraction of boiled BL21 *E. coli* supernatant separated with a NAP-10 column. Extraction of crude phospholipids from BL21 *E. coli* cells was performed as described previously [53].

Table 3 Phospholipid effect on HisBchM activity

Additives of crude and commercial phospholipids were assayed over a variety of concentrations with the optimal amounts stated based on the greatest stimulatory effect in a 100 μl assay (see Supplementary Figure 1 at http://www.BiochemJ.org/bj/406/bj4060469add.htm for an example). Assays were as described in the Experimental section, with the concentrations and any variations stated in the Table. Assays were performed for 0.5 min (DPPG) or 10 min for the remaining phospholipids and compared with a control (assigned a value of 100 % activity) conducted in parallel.

Additive	pH	Mg-proto (μM)	SAM (μM)	HisBchM (μM)	Amount additive (μg)*	% Control
Pg, mixed alkyl chain	8.5	2	250	0.018	2	1035
Ps, mixed alkyl chain	8.5	2	250	0.018	5	865
Pe, mixed alkyl chain	8.5	2	250	0.018	20	139
Dioleoyl ($C_{18:1}$)$_2$ pg (DOPG)	8.5	2	77	0.041	5	442
Palmitoyl-oleoyl ($C_{16:0,18:1}$) pg (POPG)	8.5	2	77	0.041	1	494
Dipalmitoyl ($C_{16:0}$)$_2$ pg (DPPG)	8.0	0.5	80	0.05	4	81

*Additives were used over a variety of concentrations with the optimal amounts stated here based on the greatest stimulatory effect.

Pg (phosphatidylglycerol) is the main phospholipid present in *R. capsulatus* [56] and a mixed alkyl chain pg was initially tested for its effect on HisBchM activity and found to have a 10-fold stimulatory effect. Two other phospholipids were tested with variations in the polar head group, ps (phosphatidylserine) and pe (phosphatidylethanolamine), with an 8-fold and 1.3-fold stimulatory effect respectively. These results seem to correlate with the polarity and charge of the phospholipid, the greatest stimulatory effect seen with the most polar negatively charged phospholipid, pg. Ps, a negatively charged phospholipid of intermediate polarity not present in significant quantities in *R. capsulatus* [56], also had a strong stimulatory effect. A comparatively marginal effect was observed with the most non-polar neutral phospholipid tested, pe. This appears to coincide with the known phospholipid composition of *R. capsulatus*, which is mainly composed of pg, whether grown heterotrophically or photosynthetically. It has also been shown that there is a large increase in the amount of pg in photosynthetically grown cells (62.5 %) compared with heterotrophic growth (39.3 %) together with a large decrease in pe (33.8 to 18.7 %) [56]. Variant pgs were tested with differing alkyl chains. There was little difference in activity between two unsaturated alkyl chains, dioleoyl ($C_{18:1}$)$_2$ phosphatidylglycerol (DOPG) or one, POPG with both exhibiting a 4–5-fold effect on HisBchM; however, no stimulatory effect was observed with a saturated alkyl chain phospholipid, dipalmitoyl ($C_{16:0}$)$_2$ phosphatidylglycerol (DPPG) highlighting the importance of the single double bond or the C_{18} chain. The oleoyl ($C_{18:1}$) chain might be important since it is the major phospholipid fatty acid chain length of pg in *R. capsulatus* (83.5 to 85.7 %), with the remainder being $C_{16:0}$, $C_{16:1}$ and $C_{18:0}$ [56]. The greater stimulatory effect seen with mixed pg as opposed to DOPG or POPG may suggest the need for a variable alkyl chain length (possibly $C_{16:1}$ or $C_{18:0}$).

Dilution of HisBchM with a constant concentration of DOPG resulted in a protein-concentration-dependent production of MgPE (see Supplementary Figure 2 at http://www.BiochemJ.org/bj/406/bj4060469add.htm). It is not surprising that phospholipids are associated with HisBchM from *R. capsulatus* in the present study, since the enzyme activity has been localized in chromatophores and membrane fragments in *R. spheroides* [20,57] and a putative transmembrane domain has also been identified [30]. Since phospholipids are prevalent in membrane proteins and required for structural integrity and enzymatic activity [55], it is likely that the BchM protein from *R. capsulatus* is membrane-bound *in vivo*.

Physical properties of HisBchM

Phospholipids had a significant effect on the aggregation state of HisBchM *in vitro* using size-exclusion chromatography (see Supplementary Figure 3 at http://www.BiochemJ.org/bj/406/bj4060469add.htm). Without phospholipids the majority of purified 29 kDa HisBchM existed as a high molecular mass aggregate or multimer. This is in contrast with pure ChlM protein from *Synechocystis*, which exists solely as a monomer [25]. The addition of a crude phospholipid preparation from *E. coli* shifted the elution profile of the protein to lower molecular mass complexes, suggesting a disaggregation process. A more profound effect was observed on the aggregation state of HisBchM with the addition of pg (mixed alkyl chain) which resulted in a large proportion of the protein eluting as an apparent monomer. Analysis of the CD spectrum of this solubilised HisBchM (see Supplementary Figure 4 at http://www.BiochemJ.org/bj/406/bj4060469add.htm) using CDPro program [58], indicated that the majority of protein is α-helical 56 %) with a significant proportion of disordered structure (20 %) and some β-sheet (16 %).

Effect of magnesium–chelatase on methyltransferase activity

It has been reported previously that the BchH subunit of the magnesium–chelatase stimulates the activity of the BchM methyltransferase [36]. In the light of the effect of phospholipids stimulating and stabilizing the HisBchM we decided to re-examine this effect using purified magnesium-chelatase subunits. Formation of the magnesium–chelatase complex requires magnesium ions and ATP and so the effect of magnesium ions on methyltransferase activity was also tested. Increasing magnesium ion concentrations caused a decrease in methyltransferase activity, possibly

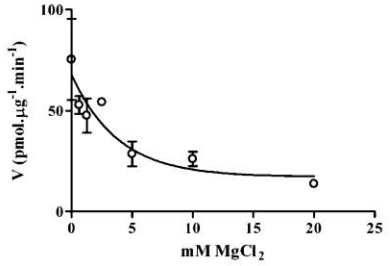

Figure 2 Effect of $MgCl_2$ on HisBchM activity

Assays were performed in triplicate with the following concentrations: 50 mM Tricine/NaOH (pH 8.0), 1 mM DTT, 100 μM SAM, 0.4 μM Mg-proto, 0.1 μM HisBchM, 2.4 mM glycerol and variable $MgCl_2$ (0, 0.625, 1.25, 2.5, 5, 10, 20 mM) for 0.5 min. The results are presented as means $\pm$ S.D.

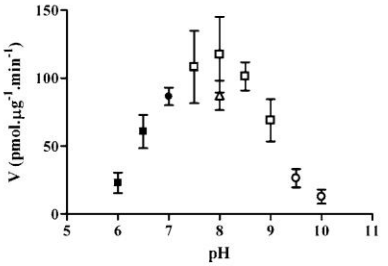

Figure 3 Optimal pH range for HisBchM activity

The following buffers were used: ○ $NaHCO_3$, □ Tris/HCl, △ Tricine/NaOH, ● MOPS/NaOH, ■ MES/NaOH. The assay consisted of 40 mM buffer, 1 mM DTT, 2.4 mM glycerol, 0.4 μM Mg-proto, 100 μM SAM and 0.1 μM HisBchM for 0.5 min. The results are presented as means $\pm$ S.D. for assays performed in triplicate

Table 4 HisBchH effect on methyltransferase activity

A 5 min pre-incubation of HisBchH with HisBchM was performed at room temperature prior to the assay. Assays were performed for 0.5 min with the following concentrations: 50 mM Tricine/NaOH (pH 8.0), 1 mM DTT, 100 μM SAM, 0.4 μM Mg-proto, 0.1 μM HisBchM, 51 mM glycerol and 0.54 mM $MgCl_2$. The results are presented as means $\pm$ S.D.

HisBchH (μM)	H:M	V (pmol/min per μg of protein)
0	0	74.6 $\pm$ 3.5
0.0071	0.074	65.6 $\pm$ 4.8
0.021	0.22	58.6 $\pm$ 6.7
0.063	0.67	67.5 $\pm$ 1.2
0.19	2.0	60.5 $\pm$ 6.6
0.57	6.0	43.6 $\pm$ 15

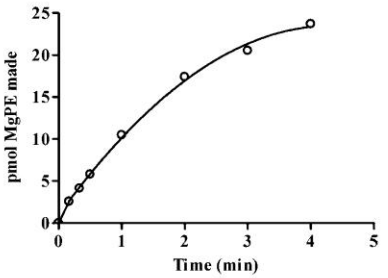

Figure 4 Linearity of the HisBchM assay

The following time points were used: 0, 10, 20, 30, 60, 120, 180 and 240 s, with the following assay components: 50 mM Tricine/NaOH (pH 8.2), 1 mM DTT, 0.25 μM Mg-proto, 75 μM SAM, 0.1 μM HisBchM, 3.1 μM DOPG and 2.2 mM glycerol.

due to aggregation of the enzyme Figure 2). The HisBchH appears to slightly inhibit the methyltransferase activity using a limiting or excess molar amount of HisBchH compared with HisBchM (Table 4) and a low magnesium chloride concentration (0.54 mM). In addition the combination of other magnesium-chelatase subunits and BSA were also tested for stimulation of methyltransferase activity (see Supplementary Figure 5 at http://www.BiochemJ.org/bj/406/bj4060469add.htm). At a low magnesium chloride concentration (0.54 mM) there is little effect of these proteins on methyltransferase activity. Higher magnesium ion concentrations (3.8 mM) inhibited HisBchM activity in the presence or absence of magnesium–chelatase subunits or BSA. At 3.8 mM magnesium chloride and 1.01 mM ATP an active magnesium–chelatase complex was formed according to a positive magnesium–chelatase assay independent of methyltransferase (results not shown), and the effect on methyltransferase was the same as without ATP. The idea of a physical interaction was proposed by Gorchein [35], with an *in vivo* study using *R. spheroides*. Much later it has been shown that crude BchM from *R. spheroides* was stimulated by crude BchH expressed in *E. coli* [36]. It has been proposed that BchH (with Mg-proto bound) is the real substrate for BchM [38]. A stimulatory effect of *Synechocystis* ChlH on *Synechocystis* ChlM methyltransferase activity has been shown with a molar excess of ChlH on a millisecond time scale [38]; however, no increased activity was seen with purified protein from *Synechocystis* over 30 min [37], highlighting the speed of the interaction. This might be the reason we do not see a direct stimulatory effect of HisBchH on HisBchM.

Enzymatic mechanism

Prior to performing detailed kinetic studies, preliminary experiments were performed to optimize the assay conditions including determining the optimal pH and linearity of the assay. The pH range for active HisBchM is reasonably broad and peaks at approx. 8.0 although pH 7.5–8.5 are also within the error range (Figure 3). There also seems to be a slight preference for Tris/HCl buffer over Tricine/NaOH. A previous study with chromatophores of *R. spheroides* showed an optimal pH value of 8.4 using Tris/HCl [20]. The HisBchM methyltransferase assay was optimized and was shown to give a constant rate of product formation up to approx. 70 % conversion to MgPE, which occurred after $\sim$ 100 s (Figure 4). There is a rapid formation of MgPE product, even after 10 s, and previous recent quenched flow analysis using the BchM orthologue, ChlM, from *Synechocystis* indicated the presence of an intermediate [24]. We were unable to observe this intermediate in this system despite using a similar HPLC method for detection.

Kinetic analysis was performed by varying one of the substrates, while keeping the second substrate constant. Analysis of the kinetic data was performed by GraphPad Prism version 4.00, GraphPad Software (San Diego, CA, U.S.A.). Non-linear regression and the two models, sequential [$Y = V_{max}AX/(AU + K_aX + K_bA + K_{ia}K_b)$], and ping-pong [$Y = V_{max}AX/(AX + K_aX + K_bA)$] were tested [59]. The data clearly showed a sequential

Table 5 Summary of kinetic data for biologically active substrates

Kinetic data for metalloporphyrin (MP) substrates. Assays were performed in triplicate with graphical data shown in Supplementary Figures 6 and 7 (http://www.BiochemJ.org/bj/406/bj4060469add.htm). Apparent K_i values for Zn-proto and Mg-deutero were determined using 250 μM SAM and previously determined constants, K_i^{SAM} 31 μM, K_m^{SAM} 45 μM and a global fit used for the V_{max} and K_m^{MP}. The following metallopophyrin concentration ranges were used: 0.0625–4 μM for Mg-deutero and 0.07–0.87 μM for Zn-proto.

Substrate	K_m^{MP} (μM)	$K_i^{Mg-proto}$ (μM)	K_m^{SAM} (μM)	K_i^{SAM} (μM)	V_{max} (pmol/min per μg)	K_{cat} (s^{-1})	K_{cat}/K_m ($M^{-1} \cdot s^{-1}$)
Mg-proto	0.11 ± 0.02	0.076 ± 0.03	45 ± 7	31 ± 7	97 ± 6	0.04	4×10^5
Zn-proto	0.08 ± 0.02	–	–	–	43 ± 2	0.018	2.3×10^5
Mg-deutero	0.06 ± 0.03	–	–	–	7.3 ± 0.3	0.003	5×10^4

Table 6 Enzymatic mechanism of HisBchM

Product inhibition of SAH (see Supplementary Figure 8 at http://www.BiochemJ.org/bj/406/bj4060469add.htm), and product inhibition of MgPE (see Supplementary Figure 9 at http://www.BiochemJ.org/bj/406/bj4060469add.htm). The results are presented as means $\pm$ S.D. N.D., not determined

Variable substrate	SAH, inhibition type	K_i^{SAH} (μM)	MgPE, inhibition type	K_i^{MgPE} (μM)
Mg-proto	Non-competitive	122 ± 11	N.D.	–
Mg-deutero	N.D.	–	Non-competitive	0.45 ± 0.03
SAM	Non-competitive	141 ± 16	Non-competitive	0.61 ± 0.06

type of mechanism ($P = 0.0015$), and the kinetic constants were determined (Table 5, and Supplementary Figures 6 and 7 at http://www.BiochemJ.org/bj/406/bj4060469add.htm) with a K_m of 44 ± 8 μM for SAM, 0.11 ± 0.02 μM for Mg-proto and V_{max} 93 ± 5 pmol/min per μg of protein. These values were comparable with previous kinetic data for SAM (20–230 μM), whereas the K_m for the porphyrin was approx. 100–400-fold lower than previous data with algal or plant BchM orthologues, 10–48 μM [19,21,25,26,29]. Although not quantitated, the K_m value of Mg-proto from *R. spheroides* has been shown previously to be much lower than plant or algal methyltransferase [22].

Product inhibition with both SAH and MgPE was performed to elucidate the reaction mechanism in terms of the order of substrate binding and product release. The following non-linear regression equations were used with GraphPad Prism: Non-competitive, $\{Y = [V_{max}X/(1 + I/K_i)]/K_m + X\}$; and Competitive, $K_m(app) = K_m[1 + I/K]$, $Y = V_{max}X/[K_m(app) + X]$. Non-competitive inhibition was seen using SAH with respect to either Mg-proto or SAM substrate (Table 6, and see Supplementary Figure 8 at http://www.BiochemJ.org/bj/406/bj4060469add.htm). Product inhibition with MgPE was performed using Mg-deutero as the substrate instead of Mg-proto which enabled separation of the MgPE inhibitor from the Mg-deutero monomethyl ester product made. Inhibition of MgPE against Mg-deutero was assumed to be the same type of inhibition expected as if Mg-proto was used as a substrate. Non-competitive inhibition was found using MgPE against either substrate, Mg-deutero or SAM (Table 6, and see Supplementary Figure 9 at http://www.BiochemJ.org/bj/406/bj4060469add.htm). This product inhibition pattern is characteristic of a random sequential-type mechanism (Figure 5), whereupon substrate binding is a random process with either Mg-proto or SAM able to bind first to the enzyme. The product release is also apparently non-ordered with either product SAH or MgPE released first from the enzyme. Also, both E–Mg-proto–SAH and E–SAM–MgPE (where E is the enzyme) form dead-end complexes and are unable to be out-competed with the substrates SAM and Mg-proto.

(Metallo)porphyrin substrate specificity of HisBchM

In addition to Mg-proto, only Zn-proto and Mg-deutero were found to be substrates for the enzyme, with no product formation detected using protoporphyrin IX, deuteroporphyrin, Cu-proto, Ni-proto, Fe(II)-proto, Fe(III)-proto, Co(II)-proto, Co(III)-proto, Mn(II)-proto and Mn(III)-proto as substrates. The Zn-proto and Mg-deutero were found to have similar K_m values to Mg-proto; however, the V_{max} values were 2-fold and 13-fold lower than Mg-proto respectively (Table 5). Previous studies showed that *R. spheroides* BchM was able to utilise the following porphyrins

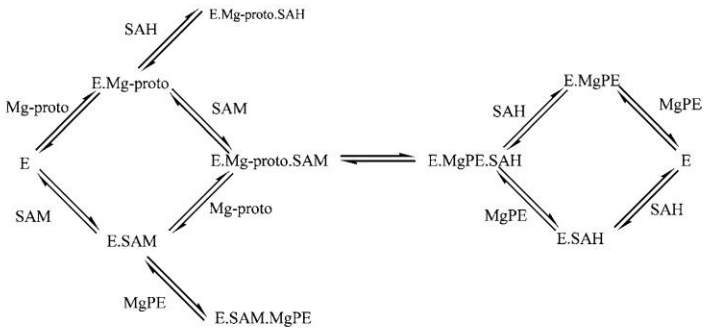

Figure 5 Random-order reaction mechanism for methyltransferase from *R. capsulatus*

Either substrate Mg-proto or SAM may bind to the enzyme E first and two dead-end complexes can exist, E–Mg-proto–SAH and E–SAM–MgPE.

Table 7 Metalloporphyrin inhibitors of HisBchM

Assays were performed in duplicate for 0.5 min with 50 mM Tricine/NaOH, pH 8.0, 1 mM DTT, 4 mM glycerol, 100 μM SAM, 0.1, 0.2, 0.3 or 0.4 μM Mg-proto, 0.06 μM HisBchM and 6.5 μM POPG, with or without 25 mM dithionite. A global fit was used to determine the kinetic parameters with the results presented as means $\pm$ S.D. N.D., not determined (refer to the text for more information).

Inhibitor used	Inhibition	Inhibition type	K_i (μM)	K_m (μM)	V_{max} (pmol/min per μg)
Protoporphyrin IX	No	–	–	–	–
Deuteroporphyrin	No	–	–	–	–
Cu-proto	No	–	–	–	–
Ni-proto	No	–	–	–	–
Fe(III)-proto	No	–	–	–	–
Fe(II)-proto	No	–	–	–	–
Co(III)-proto	No	–	–	–	–
Co(II)-proto	Yes	Competitive	0.65 ± 0.12	0.22 ± 0.05	234 ± 26
Mn(III)-proto	Yes	Non-competitive	2.7 ± 0.4	0.12 ± 0.03	193 ± 15
		Uncompetitive	1.6 ± 0.3	0.15 ± 0.04	213 ± 21
Mn(II)-proto	Yes	N.D.	N.D.	N.D.	N.D.

as substrates of decreasing efficiency with respect to Mg-proto (100 %): Ca-proto (73 %), Zn-proto (57 %), Mg-deutero (23 %) and Mg-meso (20 %) [20]. This shows the importance of both the vinyl group and the metal for optimal catalytic activity. It has been shown previously that Zn-proto is a physiological substrate in *Zea mays* with approximately 26–44 % efficiency of Mg-proto [60]. Several metalloporphyrins were not substrates with BchM from *R. spheroides*, which included Mn-proto, Fe-proto, Cu-proto, protoporphyrin IX and deuteroporphyrin [20]. There seems to be a correlation between the metalloporphyrin co-ordinate structure and HisBchM activity. Depending upon the metal ion inserted into the porphyrin, metalloporphyrins may have zero, one or two addition axial ligands (e.g. water molecules) bound to the metal atom [61]. The metalloporphyrins that exhibited activity (Mg-proto, Zn-proto and Mg-deutero) have one ligand bound to the metal in the tetrapyrrole nucleus forming a 5-co-ordinate square-pyramidal structure. Ni-proto and Cu-proto are stable with no ligands bound and have a square-planar 4-co-ordinate structure. Mn-proto, Co-proto and Fe-proto can exist as either octahedral 6-co-ordinate or 5-co-ordinate structures depending on the oxidation state, environment and ligand [61]. The 5-co-ordinate square-pyramidal structures are usually distorted with one ligand bound, which may be important for initiating catalysis. The 4- or 6-co-ordinate metalloporphyrins may not be able to fit into the active-site due to the lack of an exchange ligand or an extra ligand.

(Metallo)porphyrin inhibition

The (metallo)porphyrins that were not substrates for HisBchM were tested as inhibitors (Table 7). Mg-, Zn-, Cu- and Ni-porphyrin exist in the Metal(II) oxidation state, whereas Fe-, Co-, and Mn-proto exist primarily in the Metal(III) oxidation state, which can be reduced to the Metal(II) state with dithionite and both of these forms were tested. There were no inhibitory effects of the following porphyrins up to 1 μM: protoporphyrin IX, deuteroporphyrin, Cu-proto, Ni-proto, Fe(III)-proto and Co(III)-proto. Assays involving Mn(II)-proto or Fe(II)-proto gave variable results, as the inhibitors interfered with separation and detection in the HPLC chromatography, and K_i values could not be determined and in this case the unidentified values are stated as not determined. Fe(II)-proto was not inhibitory up to 3 μM using a substrate concentration of 0.4 μM Mg-proto, whereas Mn(II)-proto was approx. 30 % inhibitory at 0.5 μM. The only strong inhibitors observed were Mn(III)-proto and Co(II)-proto, and the K_i values and inhibition type were determined. The following non-linear regression equations were used with GraphPad Prism: Non-competitive; Uncompetitive, $Y = V_{max}X/[K_m + X(1 + I/K_i)]$; and Competitive. Mn(III)-proto and Co(II)-proto gave different inhibition patterns with Mn(III)-proto showing uncompetitive or non-competitive inhibition (no significant difference was found with either inhibition type) and K_i 1.6–2.7 μM, with Co(II)-proto seemingly being competitive (K_i 0.65 μM). Previous data with *R. spheroides* has shown that both Fe-proto and Mn-proto are strong inhibitors with Fe(III)-proto seemingly a non-competitive inhibitor. Cu-proto was a weak inhibitor, although much higher concentrations of the porphyrin inhibitors were used (110–240 μM and 125 μM Mg-proto substrate) [20] compared with our assays (0.5–3 μM inhibitor and 0.1–0.4 μM Mg-proto).

One of the common features of the metalloporphyrins which act as either substrates or inhibitors is that these metalloporphyrins prefer to have five co-ordination bonds with the metal and adopt a geometry in which the metal ion forms a square pyramidal structure with the metal out of the average plane of the porphyrin macrocycle in the direction of the fifth ligand. Fe(II)-proto is an exception as it is not a substrate or inhibitor but has five co-ordination bonds with the metal, which can be in or out of plane with the porphyrin depending on the ligand and spin state of the metal. Of the remaining metalloporphyrins that were not substrates or inhibitors most generally prefer to have four or six co-ordination bonds with the metal ion remaining in the plane of the macrocycle. Zn(II) and Mg(II) derivatives of metalloporphyrins have the metal ion between 0.35 and 0.4 Å (1 Å = 0.1 nm) out of plane of the porphyrin macrocycle (see [62] for review) and the fifth co-ordination bond to either an N or O group on the fifth ligand. This compares with known 5-co-ordinate Co(II) porphyrin structures in which the metal ion is 0.15 Å out of plane of the macrocycle, while similar 5-co-ordinate Mn(II) and Mn(III) metalloporphyrins have the metal ion between 0.5 and 0.74 Å out of plane of the macrocycle [62]. It appears that catalysis can only occur when the metal ion is out of plane from the macrocycle over a very narrow range, and thus the metal ion–ligand bond is important in the correct positioning of the porphyrin for methylation.

Conclusion

Phosphatidylglycerol plays an important role for BchM solubility, stability, and enzymatic activity. This seems to be synonymous with a requirement of this phospholipid for the bacteriochlorophyll biosynthetic pathway in *R. capsulatus* and it suggests a role for it in the regulation of *bchM* activity *in vivo*. No stimulation of activity was observed with magnesium–chelatase subunits but it is important to note that it is still possible that the BchM and magnesium–chelatase subunits could interact *in vitro* and *in vivo* even though there is no effect on the activity of BchM.

We would like to thank David Bollivar (Department of Biology, Illinois Wesleyan University, Bloomington, IL, U.S.A.) for supplying the clone of the *R. capsulatus* BchM and Professor G.D. Markham (Fox Chase Cancer Center, Philadelphia, PA, U.S.A.) for the SAM-synthetase expression clone. Part of this work was supported by a Macquarie University Research Development Grant.

REFERENCES

1 Gregor, J. and Klug, G. (1999) Regulation of bacterial photosynthesis genes by oxygen and light. FEMS Microbiol. Lett. **179**, 1–9

2 Biel, A. J. and Marrs, B. L. (1983) Transcriptional regulation of several genes for bacteriochlorophyll biosynthesis in *Rhodobacter capsulatus*. J. Bacteriol. **156**, 686–694
3 Zsebo, K. M. and Hearst, J. E. (1984) Genetic-physical mapping of a photosynthetic gene cluster from *R. capsulata*. Cell **37**, 937–947
4 Taylor, D. P., Cohen, S. N., Clark, W. G. and Marrs, B. L. (1983) Alignment of genetic and restriction maps of the photosynthesis region of the *Rhodopseudomonas capsulata* chromosome by a conjugation-mediated marker rescue technique. J. Bacteriol. **154**, 580–590
5 Yen, H.-C. and Marrs, B. L. (1976) Map of genes for carotenoid and bacteriochlorophyll biosynthesis in *Rhodopseudomonas capsulata*. J. Bacteriol. **126**, 619–629
6 Marrs, B. (1981) Mobilization of the genes for photosynthesis from *Rhodopseudomonas capsulata* by a promiscuous plasmid. J. Bacteriol. **146**, 1003–1012
7 Alberti, M., Burke, D. H. and Hearst, J. E. (1995) Structure and sequence of the photosynthetic gene cluster. In Anoxygenic Photosynthetic Bacteria, (Blankenship, R. E., Madigan, M. T. and Bauer, C. E., eds), pp.1083–1106, Kluwer Academic Publishing, Amsterdam
8 Yang, Z. and Bauer, C. E. (1990) *Rhodobacter capsulatus* genes involved in early steps of the bacteriochlorophyll biosynthetic pathway. J. Bacteriol. **172**, 5001–5010
9 Bollivar, D. W., Jiang, Z.-Y., Bauer, C. E. and Beale, S. I. (1994) Heterologous expression of the BchM gene product from *Rhodobacter capsulatus* and demonstration that it encodes *S*-adenosyl-L-methionine:Mg-protoporphyrin IX methyltransferase. J. Bacteriol. **176**, 5290–5296
10 Gibson, L. S. D. and Hunter, C. N. (1994) The bacteriochlorophyll biosynthesis gene, bchM, of *Rhodobacter sphaeroides* encodes *S*-adenosyl:Mg protoporphyrin IX methyltransferase. FEBS Lett. **352**, 127–130
11 Beale, S. I. (1999) Enzymes of chlorophyll biosynthesis. Photosynthesis Res. **60**, 43–73
12 Beale, S. I. and Weinstein, J. D. (1990) Tetrapyrrole metabolism in photosynthetic organisms. In Biosynthesis of Heme and Chlorophylls (Dailey, H.A., ed.), pp. 287–391, McGraw-Hill Publishing, New York
13 Willows, R. D. (2003) Biosynthesis of chlorophylls from protoporphyrin IX. Natural Products Reports **20**, 1–16
14 Bollivar, D. W. (2006) Recent advances in chlorophyll biosynthesis. Photosynthesis Res. **89**, 1–22
15 Bollivar, D. W. (2003) Intermediate steps in chlorophyll biosynthesis methylation and cyclization. In The Porphyrin Handbook, Chlorophylls and Bilins: Biosynthesis, Synthesis, and Degradation (Kadish, K.M., Smith, K.M., Guilard, R., eds), pp. 49–69, Academic Press, Sydney
16 Pontier, D., Albrieux, C., Joyard, J., Lagrange, T. and Block, M. A. (2007) Knock-out of the magnesium protoporphyrin IX methyltransferase gene in *Arabidopsis*: effects on chloroplast development and on chloroplast-to-nucleus signaling. J. Biol. Chem. **282**, 2297–2304
17 Nott, A., Jung, H.-S., Koussevitzky, S. and Chory, J. (2006) Plastid-to-nucleus retrograde signaling. Ann. Rev. Plant Biol. **57**, 739–759
18 Ellsworth, R. K. and Dullaghan, J. P. (1972) Activity and properties of *S*-adenosyl-L-methionine:magnesium-protoporphyrin IX methyltransferase in crude homogenates from wheat seedlings. Biochim. Biophys. Acta **268**, 327–333
19 Ellsworth, R. K., Dullaghan, J. P. and St Pierre, M. E. (1974) The reaction mechanism of *S*-adenosyl-L-methionine:magnesium protoporphyrin IX methyltransferase of wheat. Photosynthetica **8**, 375–383
20 Gibson, K. D., Neuberger, A. and Tait, G. H. (1963) Studies on the biosynthesis of porphyrin and bacteriochlorophyll by *Rhodopseudomonas spheroides*. Biochem. J. **88**, 325–334
21 Hinchigeri, S. B., Chan, J. C.-S. and Richards, W. R. (1981) Purification of *S*-adenosyl-L-methionine:magnesium protoporphyrin IX methyltransferase by affinity chromatography. Photosynthetica **15**, 351–359
22 Hinchigeri, S. B., Nelson, D. W. and Richards, W. R. (1984) The purification and reaction mechanism of *S*-adenosyl-L-methionine:magnesium protoporphyrin IX methyltransferase from *Rhodopseudomonas sphaeroides*. Photosynthetica **18**, 168–178
23 Hinchigeri, S. B. and Richards, W. R. (1982) The reaction mechanism of *S*-adenosyl-L-methionine:magnesium protoporphyrin IX methyltransferase from *Euglena gracilis*. Photosynthetica **16**, 554–560
24 Shepherd, M. and Hunter, C. N. (2004) Transient kinetics of the reaction catalysed by magnesium protoporphyrin IX methyltransferase. Biochem. J. **382**, 1009–1013
25 Shepherd, M., Reid, J. D. and Hunter, C. N. (2003) Purification and kinetic characterization of the magnesium protoporphyrin IX methyltransferase from *Synechocystis* PCC6803. Biochem. J. **371**, 351–360
26 Shieh, J., Miller, G. W. and Psenak, M. (1978) Properties of *S*-adenosyl-L-methionine magnesium-protoporphyrin IX methyltransferase from barley. Plant Cell Physiol. **19**, 1051–1059
27 Yee, W. C., Eglsaer, S. J. and Richards, W. R. (1989) Confirmation of a ping-pong mechanism for *S*-adenosyl-L-methionine:magnesium protoporphyrin methyltransferase of etiolated wheat by an exchange reaction. Biochem. Biophys. Res. Commun. **162**, 483–490
28 Smith, C. A., Suzuki, J. Y. and Bauer, C. E. (1996) Cloning and characterization of the chlorophyll biosynthesis gene *chlM* from *Synechocystis* PCC6803 by complementation of a bacteriochlorophyll biosynthesis mutant of *Rhodobacter capsulatus*. Plant Mol. Biol. **30**, 1307–1314
29 Ebbon, J. G. and Tait, G. H. (1969) Studies on *S*-adenosyl-magnesium protoporphyrin methyltransferase in *Euglena gracilis* strain Z. Biochem. J. **111**, 573–582
30 Block, M. A., Tewari, A. K., Albrieux, C., Maréchal, E. and Joyard, J. (2002) The plant *S*-adenosyl-L-methionine:Mg-protoporphyrin IX methyltransferase is located in both envelope and thylakoid chloroplast membranes. Eur. J. Biochem. **269**, 240–248
31 Walker, C. J. and Willows, R. D. (1997) Mechanism and regulation of Mg-chelatase. Biochem. J. **327**, 321–333
32 Willows, R. D. and Hansson, M. (2003) Mechanism, structure, and regulation of magnesium chelatase. In The Porphyrin Handbook (Kadish, K.M., Smith, K.M. and Guilard, R., eds), pp. 1–47, Academic Press, Sydney
33 Vale, R. D. (2000) AAA proteins: lords of the ring. J. Cell Biol. **150**, F13–F19
34 Willows, R. D., Gibson, L. C. D., Kanangara, G. C., Hunter, C. N. and von Wettstein, D. (1996) Three separate proteins constitute the magnesium chelatase of *Rhodobacter sphaeroides*. Eur. J. Biochem. **235**, 438–443
35 Gorchein, A. (1972) Magnesium protoporphyrin chelatase activity in *Rhodopseudomonas sphaeroides*: studies with whole cells. Biochem. J. **127**, 97–106
36 Hinchigeri, S. B., Hundle, B. and Richards, W. R. (1997) Demonstration that the BchH protein of *Rhodobacter capsulatus* activates *S*-adenosyl-methionine:magnesium protoporphyrin IX methyltransferase. FEBS Lett. **407**, 337–342
37 Jensen, P. E., Gibson, L. C. D., Shepherd, F., Smith, V. and Hunter, C. N. (1999) Introduction of a new branchpoint in tetrapyrrole biosynthesis in *Escherichia coli* by co-expression of genes encoding the chlorophyll-specific enzymes magnesium chelatase and magnesium protoporphyrin methyltransferase. FEBS Lett. **455**, 349–354
38 Shepherd, M., McLean, S. and Hunter, C. N. (2005) Kinetic basis for linking the first two enzymes of chlorophyll biosynthesis. FEBS J. **272**, 4532–4539
39 Alawady, A., Reski, R., Yaronskaya, E. and Grimm, B. (2005) Cloning and expression of the tobacco CHLM sequence encoding Mg protoporphyrin IX methyltransferase and its interaction with Mg chelatase. Plant Mol. Biol. **57**, 679–691
40 Alawady, A. E. and Grimm, B. (2005) Tobacco Mg protoporphyrin IX methyltransferase is involved in inverse activation of Mg porphyrin and protoheme synthesis. Plant J. **41**, 282–290
41 Bradford, M. M. (1976) A rapid and sensitive method for the quantitation of microgram quantities of protein utilizing the principle of protein-dye binding. Anal. Biochem. **72**, 248–254
42 Willows, R. D. and Beale, S. I. (1998) Heterologous expression of the *Rhodobacter capsulatus* BchI, D and H genes that encode magnesium chelatase subunits and characterization of the reconstituted enzyme. J. Biol. Chem. **273**, 34206–34213
43 Reference deleted
44 Boyle, S. M., Markham, G. D., Hafner, E. W., Wright, J. M., Tabor, H. and Tabor, C. W. (1984) Expression of the cloned genes encoding the putrescine biosynthetic enzymes and methionine adenosylmethyltransferase of *Escherichia coli speA, speB, speC* and *metK*. Gene **30**, 129–136
45 Markham, G. D., Hafner, E. W., Tabor, C. W. and Tabor, H. (1980) *S*-Adenosylmethionine synthetase from *Escherichia coli*. J. Biol. Chem. **255**, 9082–9092
45a Schägger, H. and von Jagow, G. (1987) Tricine-sodium dodecyl sulfate-polyacrylamide gel electrophoresis for the separation of proteins in the range from 1 to 100 kDa. Anal. Biochem. **166**, 368–379
46 Fuhrhop, J. and Granick, S. (1971) Magnesium protoporphyrin dimethyl ester and the dipotassium salt of magnesium protoporphyrin. Biochemical Preparations **13**, 55–58
47 Falk, J. E. (1964) Laboratory methods. In Porphyrins and Metalloporphyrins: Their General, Physical And Coordination Chemistry, And Laboratory Methods, pp. 135–141, Elsevier Publishing Company, New York
48 Brisbin, D. A. and Richards, G. D. (1972) Kinetics of the reaction of some first-row transition metals with protoporphyrin IX dimethyl ester. Inorg. Chem. **11**, 2849–2851
49 Karger, G. A., Reid, J. D. and Hunter, C. N. (2001) Characterization of the binding of the deuteroporphyrin IX to the magnesium chelatase H subunit and spectroscopic properties of the complex. Biochemistry **40**, 9291–9299
50 Dalziel, K. (1959) Porphyrins and related compounds. In Data for Biochemical Research (Dawson, R.M. C., Elliott, D.C., Elliott, W.H. and Jones, K.M., eds), pp. 134, Oxford University Press, London
51 Loach, P. A. and Calvin, M. (1963) Oxidation states of manganese hematoporphyrin IX in aqueous solution. Biochemistry **2**, 361–371

52 Ellsworth, R. K. and Murphy, S. J. (1978) Enzymatic preparation of Mg-protoporphyrin IX monomethyl ester. Photosynthetica **12**, 81–82
53 Osborn, M. J. and Rothfield, L. I. (1966) Formation of lipopolysaccharide in mutant strains of *Salmonella typhimurium*. Methods Enzymol. **8**, 456–466
54 Burton, K. (1959) Spectral data and pK values for purines, pyrimidines, nucleosides and nucleotides. In Data for Biochemical Research. (Dawson, R.M.C., Elliott, D.C., Elliott, W.H. and Jones, K.M., eds), pp. 74, Oxford University Press, London
55 Opekarová, M. and Tanner, W. (2003) Specific lipid requirements of membrane proteins: a putative bottleneck in heterologous expression. Biochim. Biophys. Acta **1610**, 11–22
56 Russell, N. J. and Harwood, J. L. (1979) Changes in the acyl lipid composition of photosynthetic bacteria grown under photosynthetic and non-photosynthetic conditions. Biochem. J. **181**, 339–345
57 Tait, G. H. and Gibson, K. D. (1961) The enzymic formation of magnesium protoporphyrin monomethyl ester. Biochim. Biophys. Acta **52**, 614–616
58 Sreerama, N. and Woody, R. W. (2000) Estimation of protein secondary structure from circular dichroism spectra: comparison of CONTIN, SELCON, and CDSSTR methods with an expanded reference set. Anal. Biochem. **287**, 252–260
59 Cleland, W. W. (1963) The kinetics of enzyme-catalyzed reactions with two or more substrates or products. I. Nomenclature and rate equations. Biochim. Biophys. Acta **67**, 104–137
60 Radmer, R. J. and Bogorad, L. (1967) *S*-adenosyl-L-methionine:magnesium protoporphyrin methyltransferase, an enzyme in the biosynthetic pathway of chlorophyll in *Zea mays*. Plant Physiol. **42**, 463–465
61 Falk, J. E. (1964) Further coordination by metalloporphyrins. In Porphyrins and Metalloporphyrins: Their General, Physical And Coordination Chemistry, And Laboratory Methods, pp. 41–66, Elsevier Publishing Company, New York
62 Scheidt, W. R. (2000) Systematics of the stereochemistry of porphyrins and metalloporphyrins. In The Porphyrin Handbook (Kadish, K. M., Smith, K. M. and Guilard, R., eds), pp. 49–112, Academic Press, Sydney

Received 26 February 2007/21 May 2007; accepted 26 June 2007
Published as BJ Immediate Publication 26 June 2007, doi:10.1042/BJ20070284

4.3 Supplementary data

BJ www.biochemj.org

BJ Structure

Supplementary Figure 1: Phospholipid titration effect on HisBchM activity

DOPG was titrated into the HisBchM assay. The assay was composed of 50 mM Tris-HCl pH 8.5, 1 mM DTT, 2 µM Mg-proto, 77 µM SAM, 0.04 µM HisBchM, 14 mM glycerol for 10 min. A relative activity of one hundred percent was assigned with no phospholipid present. Assays contained 0, 0.25, 0.5, 1, 2, 5, 10, 20 µg of DOPG in a 100 µl assay.

Supplementary Figure 2: Linearity of the HisBchM assay with dioleoyl ($C_{18:1}$)$_2$ phosphatidylglycerol (DOPG)

Assays were performed in triplicate with error bars expressed as a standard deviation. The assay consisted of 50 mM Tricine-NaOH pH 8.2, 1 mM DTT, 96.5 mM glycerol, 2 µM Mg-proto, 75 µM SAM, 3.1 µM DOPG for 10 min with variable enzyme concentrations; 0.01, 0.02, 0.04, 0.08, 0.16, 0.28 µM.

Supplementary Figure 3: Size-exclusion chromatography of purified HisBchM

This involved a Superose 12 3.2/30 column (GE Healthcare Biosciences) at 60 µl.min^{-1} using 10 mM Tris-HCl pH 7.8, 1 mM DTT. The following injections were performed in a final volume of 100 µl; ○ HisBchM alone (0.28 µg); □ HisBchM (0.28 µg) with 134 µg crude phospholipids (from *E.Coli*); Δ HisBchM (1.8 µg) with 4.65 µg pg (mixed chain). Fractions (100 µl) were collected and assayed with 50 mM Tris-HCl pH 8.5, 1 mM DTT, 1-2 µM Mg-proto, 100 µM SAM, for 10 min. The most active fraction was assigned a relative activity of one hundred percent. Protein standards were used with their respective elution times; Blue dextran (2000 kDa) at 1.14 ml, BSA (66 kDa) and ovalbumin (43 kDa) at 1.44-1.46 ml, chymotrypsin (25 kDa) at 1.99 ml, RNase A (13.7 kDa) at 2.13 ml. The approximate structural forms of HisBchM were denoted as monomer, dimer, multimer, and a presumed aggregate species.

Supplementary Figure 4: CD spectrum of HisBchM in the presence of pg (mixed chain)

Spectrum was performed using a JASCO J-810 CD spectropolarimeter from 202-300 nm. The sample contained 10 mM phosphate pH 7.4, 0.25 µg.µl^{-1} pg (mixed alkyl chain), 0.01 µg.µl^{-1} HisBchM.

Supplementary Figure 5: Magnesium-chelatase effect on methyltransferase activity

Magnesium-chelatase subunits BchI, HisBchD, and HisBchH are stated as I, D, and H with HisBchM labeled M. A five minute preincubation of the subunits (ID, H, IDH or BSA) with M was performed at room temperature prior to assaying. Assays were performed in triplicate with the following concentrations, 50 mM Tricine-NaOH pH 8.0, 1 mM DTT, 100 µM SAM, 0.4 µM Mg-proto, 0.1 µM HisBchM, 31 mM glycerol, 1.3 mM urea, ± 0.4 µM HisBchH or BSA, ± 0.056 µM BchI, ± 0.013 µM HisBchD for 0.5 min. Errors are stated as standard deviations.

Supplementary Figure 6: HisBchM kinetics with variable [Mg-proto] at fixed [SAM]

(A) Varying concentrations of Mg-proto; 0.073 μM, 0.109, 0.145, 0.218, 0.291, 0.582 μM at fixed SAM; ○ 15.625 μM, □ 31.25 μM, Δ 62.5 μM, ● 125 μM, ■ 250 μM. Assays were for 0.5 min in a buffer containing 50 mM Tricine-NaOH pH 8.2, 1 mM DTT, 0.08 μM HisBchM, 2.7 mM glycerol. **(B)** Line-Weaver Burke of sequential equation. A shared value for K_i^{SAM}, V_{max}, $K_m^{Mg\text{-}proto}$, and K_m^{SAM} was used for the data analysis with a sequential fit of the data using GraphPad Prism. Assays were done in triplicate and error bars expressed as standard deviation.

Supplementary Figure 7: HisBchM kinetics with variable [SAM] at fixed [Mg-proto]

(A) Varying concentrations of SAM; 15.625 μM, 31.25, 62.5, 125, 250 μM at fixed Mg-proto; ○ 0.073 μM, □ 0.109 μM, Δ 0.145 μM, ● 0.218 μM, ■ 0.291 μM, ▲ 0.582 μM. Other assay component concentrations were identical to Supplementary Figure 6. **(B)** Line-Weaver Burke of sequential equation. A shared value for $K_i^{Mg\text{-}proto}$, V_{max} and a constant $K_m^{Mg\text{-}proto}$ of 0.11 μM and K_m^{SAM} of 44.7 μM was used for the data analysis with a sequential fit of the data using GraphPad Prism. Assays were done in triplicate and error bars expressed as standard deviation.

Supplementary Figure 8: Product inhibition with SAH

(A) Product inhibition of SAH with respect to SAM at fixed SAH concentrations; ○ 0 μM, □ 100 μM, Δ 200 μM, ● 400 μM. A constant amount of SAM substrate was used (100 μM) with varying Mg-proto concentrations; 0.1, 0.15, 0.25, 0.4 μM. **(B)** Product inhibition of SAH with respect to Mg-proto at fixed SAH concentrations; ○ 0 μM, □ 100 μM, Δ 200 μM, ●, 400 μM. A constant amount of Mg-proto substrate was used (0.25 μM) with varying SAM concentrations; 31.25, 62.5, 125, 250 μM. Assays were for 0.5 min in a buffer containing 50 mM Tricine-NaOH pH 8.0, 1 mM DTT, 12 μM POPG, 11 mM glycerol, 0.06 μM HisBchM. A shared value for K_i^{SAH} and V_{max} was used for the data analysis with non-competitive inhibition using GraphPad Prism. Assays were done in triplicate and error bars expressed as standard deviation.

Supplementary Figure 9: Product inhibition with MgPE

(A) Product inhibition of MgPE with respect to SAM at fixed MgPE concentrations; ○ 0 μM, □ 0.2 μM, Δ 0.5 μM. A constant amount of Mg-deutero substrate was used (0.25 μM) with varying SAM concentrations; 31.25 μM, 62.5 μM, 125 μM, 250 μM. **(B)** Product inhibition of MgPE with respect to Mg-deutero at fixed MgPE concentrations; ○ 0 μM, □ 0.2μM, Δ 0.5 μM. A constant amount of SAM substrate was used (100 μM) with varying Mg-deutero concentrations; 0.1, 0.15, 0.25, 0.4, 0.6, 0.8 μM. Assays were for 0.5 min for (A) and 2 min for (B) in a buffer containing 50 mM Tricine-NaOH pH 8.0,

1 mM DTT, 12 μM POPG, 11 mM glycerol, 0.135 μM HisBchM, 0.5 % v/v ethanol. A shared value for K_i^{MgPE} and V_{max} was used for the data analysis with non-competitive inhibition using GraphPad Prism. Assays were done in triplicate and error bars expressed as standard deviation.

Supplementary Figure 1

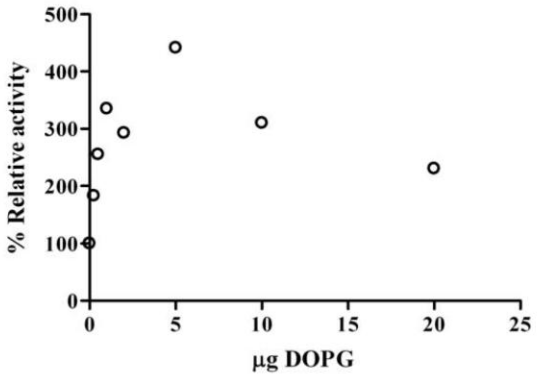

Supplementary Figure 2

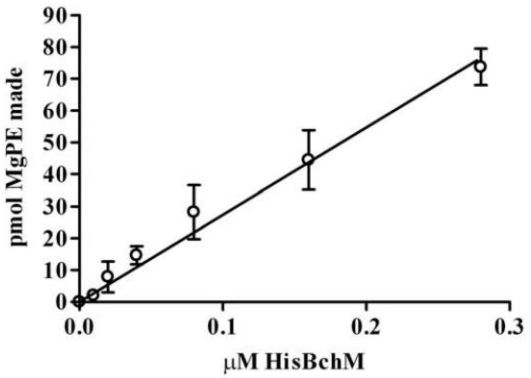

Supplementary Figure 3

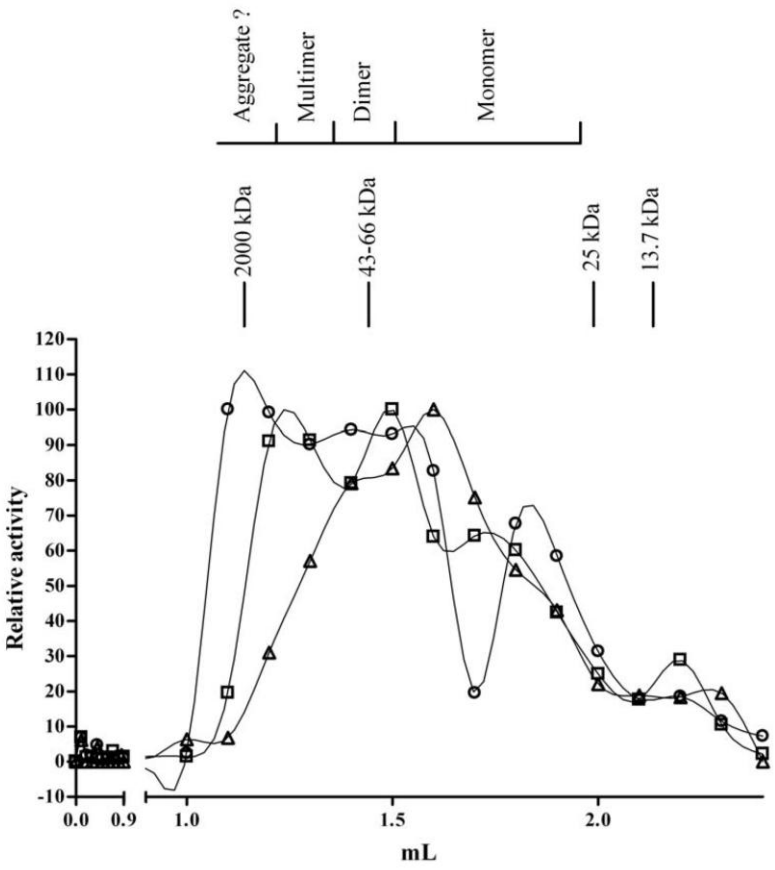

Supplementary Figure 4

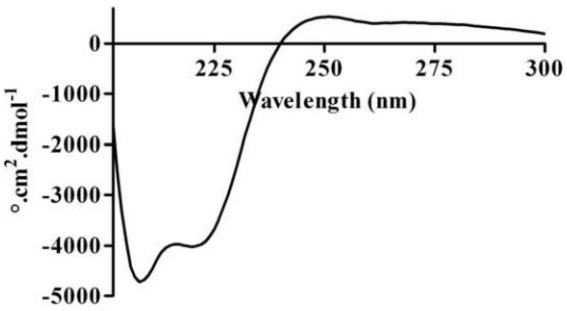

Supplementary Figure 5

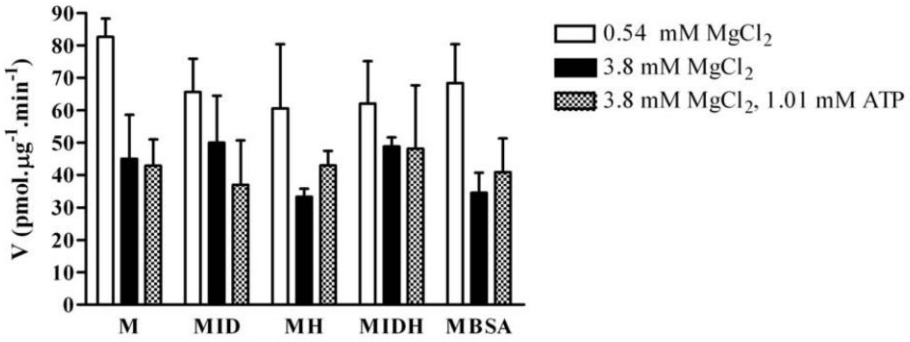

Supplementary Figure 6

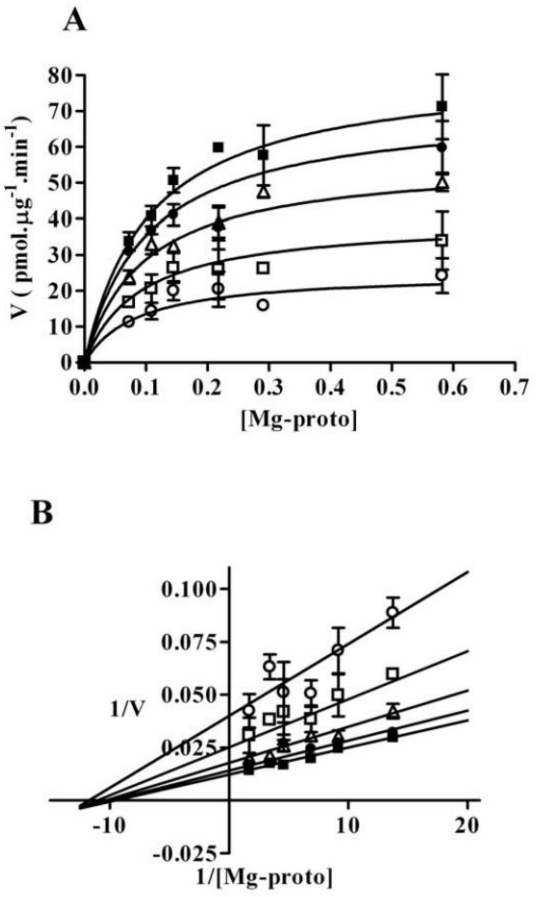

Supplementary Figure 7

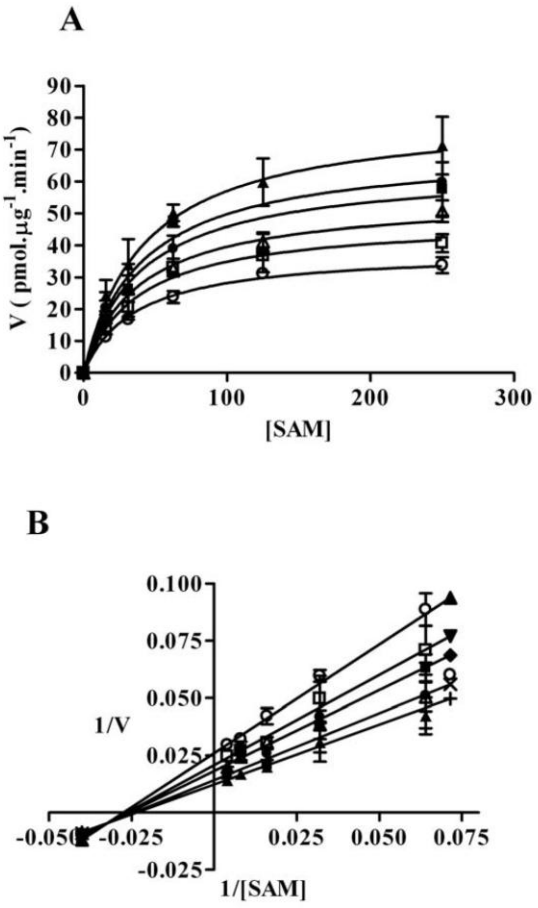

Supplementary Figure 8

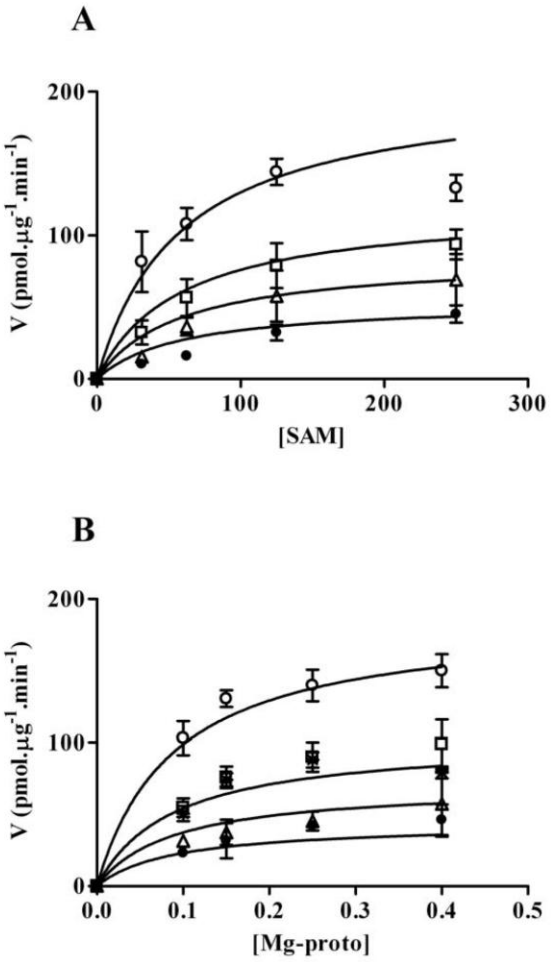

Supplementary Figure 9